Optical and Raman studies of nanocrystallinetinoxide thin films prepared by spray pyrolysis

V. K. RESHMY[a], K. G. GOPCHANDRAN[b], V. K. VAIDYAN[a,*]
[a]Department of Physics, University of Kerala, Kariavattom-695581, Kerala, India
[b]Department of Optoelectronics, University of Kerala, Kariavattom-695581, Kerala, India

Tin oxide nanocrystalline thin films were prepared using spray pyrolysis. The microstructural properties of thin films were characterized using X-ray diffraction. The particle size is found to be sensitive to substrate temperature and is in nanometric regime. Transmission spectra showed size dependent blue shift of the optical band gap which can be attributed to quantum confinement effect. In addition to Raman active and IR active modes, the micro Raman spectrum of SnO_2 thin films showed disorder activated modes and surface phonon modes due to nanosize effect.

1. Introduction

Low dimensional nanostructured materials have evoked much interest owing to their possible applications in the technological fields. The preparation of the nanosized crystallites with different morphologies provides an opportunity to explore the possible changes in their physical and chemical features with size and shape. Moreover, the possibility of tailoring the optical band gap opens up the scope for its use in optoelectronics [1,2]. The size dependence of the vibrational properties of nanosized particles is important for the basic understanding of these materials and their potential mainly in optoelectronic applications. If the particle size becomes comparable to the Bohr radius of the exciton, the ratio of surface atoms to those in the interior increases remarkably leading to the surface properties playing an important role in the properties of the material. Semiconductor nanoparticles also exhibit a change in their electronic properties relative to that of the bulk counterpart, as the size of the solid becomes smaller, the band gap becomes larger. These quantum size effects, i.e., the size tuneable material properties have stimulated great interest in both basic and applied research [4, 5]. An understanding of the size dependent phonon behaviour is, therefore, highly desirable not only because phonons influence the optical and electrical properties of solid via electron-phonon interactions, but also because of the potential for vibrational spectroscopy to become a tool for characterization of crystallite size [6].

Owing to their unique electronic, magnetic and optical properties, semiconductor nanoparticles may find wide applications in various fields such as microelectronics, photocatalysis, nonlinear optics, photoelectric chemistry, imaging science and electrooptics. Among the various semiconductor materials, SnO_2 is a pro-typical optically transparent n-type semiconductor with a wide band gap (3.62 eV at 300K), which spans a wide range of applications such as gas sensors, special coating for energy conserving "low emissivity" windows, transparent heating elements, electrodes in glass melting furnaces and antistatic coating [7,8]. SnO_2 is a promising material for short wavelength photonic devices since it has large direct band gap of 3.6 eV and a large exciton binding energy 130 meV all of which are advantages for light emitting diodes and low threshold devices. Besides, the low growth temperature and high chemical stability make SnO_2 a promising UV and blue light material. A variety of methods such as chemical vapour deposition [9], sol gel [10] sputtering [11], electron beam evaporation [12], spray pyrolysis [3,13,14] etc. are available to prepare SnO_2 thin films. Among these, spray pyrolysis is the most convenient method because of its simplicity, low cost, and ease to add doping materials. This method is also promising for high rate and mass production capability of uniform large area coatings in industry [15]. Spray pyrolysis also has been thought to produce more oxygen vacancy in tin oxide thin films [16].

Raman spectroscopy is a powerful tool for the characterization of nano-sized materials and structures. This technique is widely used for the study of phonon confinement effects, the effect of increase of local temperature, strain and substitutional effects, porosity and non-stoichiometry in different types of nanomaterials. The chemical bonds and oxygen related defects were investigated by FTIR spectrometer. The IR techniques can reveal local structure information of amorphous and poorly crystallised samples. The use of XRD and micro Raman spectroscopy together will enhance our understanding of the signals from the microstructural change and various defects in nanomaterials. For technological applications, a detailed understanding of the size, structure, composition, surface morphology, optical and vibrational properties of nanoscale SnO_2 is important.

This communication focuses on the substrate temperature dependence of grain size and nano-structural evolution of SnO_2 thin films. The change of Raman spectrum with crystal size of nano-crystalline SnO_2 thin films and phonon confinement effect on the spectrum are discussed.

2. Experimental

SnO_2 nano-crystalline thin films were prepared by the spraypyrolysis technique. 0.2M hydroethanolic solution was prepared by dissolving $SnCl_4 5H_2O$ in a mixture of absolute ethanol and high purity water in the ratio 1:1. A few drops of concentrated HCl were also added to the precursor solution. The solution was sprayed using a spray rate controlled atomiser on a glass substrate placed over a temperature controlled oven in air atmosphere. The spray rate was 55 mL/min and the solution was sprayed for a time of 60 s. The films were prepared at different substrate temperatures, 375 (Sample P), 400 (Sample Q), 430 (Sample R), 460 (Sample S), and 490^0C (Sample T).

Structural analysis of the grown films were carried out by PHILIPS Xpert X-ray diffraction spectrometer using Cu Kα radiation (λ=1.5406A^0) as an X-ray source that is equipped with Ni filter. The surface morphology of the nano-particles was studied by a scanning electron microscope (JSM 5610). The optical transmission and absorption spectroscopic measurements are performed for wavelength range 300-900nm using Shimadzu UV-Visible double beam spectroflurometer.Confocal micro Raman spectroscopy was conducted using OLYMPUS BX41 Horiba JobinYvon Confocal Raman microscope using He-Ne laser of wavelength 632.8nm. The infrared (IR) spectra of the samples were recorded in the range 400–4000cm^{-1}

on a Perkin-Elmer Fourier-transform infrared (FTIR) spectrometer using KBr pellet method.

3. Results and discussion

3.1. XRD studies

Fig. 1 shows the X-ray diffraction patterns of the film prepared at different substrate temperatures. All the peaks in the diffraction patterns except one at $2\theta = 31.61^0$ are indexed according to JCPDS card no 41-1445 of cassiterite tetragonal crystalline phase. The peak at $2\theta = 31.61^0$ is indexed according to JCPDS card no 23-1342 of SnO. In sample Q, randomly oriented SnO_2 crystalline formation starts and planes corresponding to (110), (101),(200),(211) were observed with weak intensities. The presence of broad and weak peaks indicates that SnO_2 has a very small crystalline size or that SnO_2 particles are semi crystalline in nature. As the substrate temperature increases to 460^0C the intensity corresponding to the major plane (200) gets enhanced indicating the preferential orientation of the film along (200) direction. SnO_2 films prepared at 490^0C (sample T) showed a peculiar enhanced intensity shift towards (110) plane from (200) plane indicating the influence of substrate temperature in the preferential growth of the film. The average grain size was calculated using Scherer formula,

$$D = \frac{k\lambda}{\beta cos\theta} \qquad (1)$$

where D is the mean grain size of the nanoparticles, k= 0.9, $\lambda = 1.5406\ A^0$ and β is the full width at half maximum of diffraction peaks.
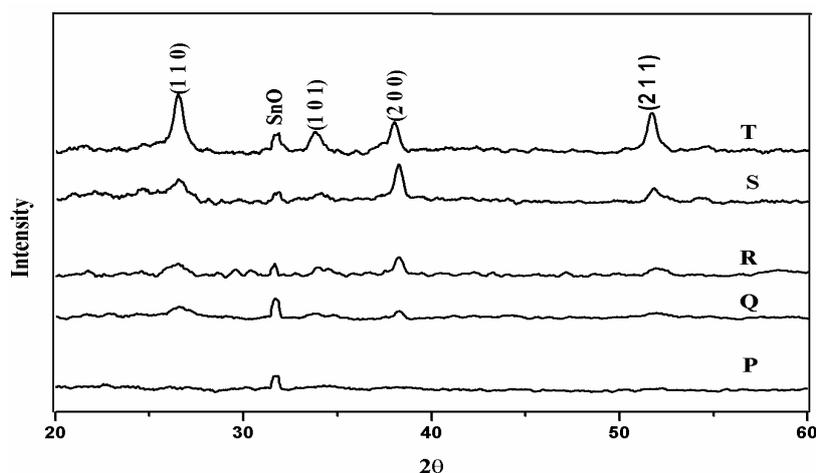

Fig. 1. XRD patterns of nanocrystallineSnO2thin films at different substrate temperatures: (P) 375^{0}C, (Q) 400^{0}C, (R) 430^{0}C, (S) 460^{0}C, (T) 490^{0}C

The as synthesized SnO_2 nanocrystalline thin film samples consist of SnO_2 grains mixed with SnO. The presence of SnO_2 and SnO in the sample may be explained as follows [17]. The forced spray flow of pentahydrated

stannic chloride ($SnCl_4 5H_2O$) and ethanol (C_2H_5OH) to the hot substrate surface induces hydrolysis reactions with the generation of radicals of tin methoxide ($Sn-(OCH_3)_x$), tin hydroxide ($Sn(OH)_x$) and other intermediate complexes

which may result in the formation of stoichiometric tin hydroxide molecules such as $Sn(OH)_4$ and $Sn(OH)_2$. The thermal decomposition at the substrate surface produces adherent SnO (insulator) and/or SnO_2 (semiconductor) films on the surface and liberates water vapour according to the following reactions.

$$Sn(OH)_4 \xrightarrow{\Delta} SnO_2 + 2H_2O \qquad (2)$$

$$Sn(OH)_2 \xrightarrow{\Delta} SnO + H_2O \qquad (3)$$

Higher substrate temperatures favour the chemical process to increase the concentration of SnO_2.

3.2. SEM studies

Fig. 2 shows scanning electron microscopic images of chemically sprayed SnO_2 thin films deposited at different temperatures. It can be seen that the morphology of the films are highly sensitive to substrate temperature. With increase in substrate temperature firstly the film becomes crystalline with morphology consisting of large grained interconnected together and with further increase in

substrate temperature to 490^0C the morphology of the film surface look like nanostructured small elongated grains. In a high temperature spray pyrolysis process, precursor solutions are sprayed onto a substrate heated to approximately 350-500ºC. The solvent is exasperated in transit and the tin oxide crystalline film is grown on the substrate surface. Substrate temperature often dictates the morphology characteristics of the film. When the sprayed particles are placed on a substrate with high surface energy, it will spread to form thin films. A thin surface film may cover the pore walls on the substrate surfaces if any in the initial stages of wetting. This is because usually the cohesive driving forces for complete spreading on the surface are much weaker than the adhesive forces and these processes will take place on different time scales, which in turn depends on the substrate temperature. Grain nucleation and growth are important phenomena in polycrystalline materials. They govern the kinetics of many phase transformations and re-crystallization processes that take place during processing. The final average grain size is directly related to the strength of the material and in general, a smaller average grain size results in a stronger material [18].
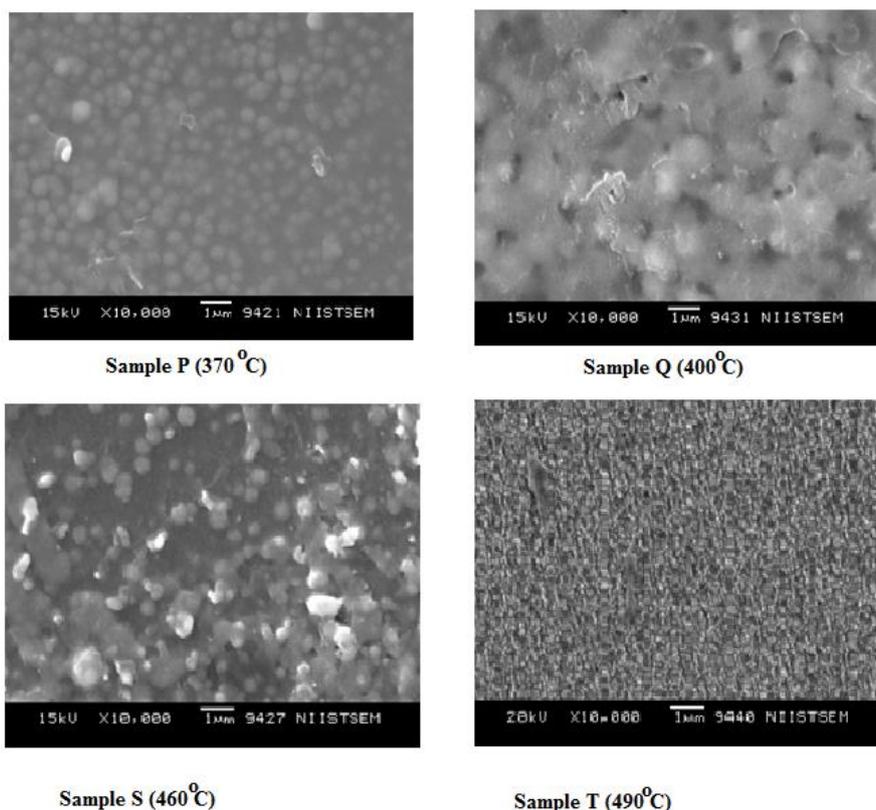

Sample P (370 ^{0}C)   Sample Q (400^{0}C)

Sample S (460^{0}C)   Sample T (490^{0}C)

Fig. 2. SEM photographs of SnO_2 thin films at different substrate temperatures

3.3. Optical studies

The transmittance spectrum of SnO_2 thin films as a function of wavelength ranging from 300 to 900 nm is shown in Fig 3. The oscillations in the spectra are caused

by optical interference arising due to difference of refractive index of films with substrate and the interference of multiple reflections originated from film and substrate surfaces. Such behaviour of transmission spectra is an evidence of the thickness uniformity of the

films [19, 20].All the films were transparent, adherent to the substrate, uniform, pinhole free and stable for long periods when kept in atmosphere. Assuming parabolic density of the states the absorption coefficient α is related to the band gap energy E_g as

$$\alpha h\nu = B(h\nu - E_g)^{\gamma} \qquad (4)$$

where$h\nu$ is the incident photon energy and η depends on the nature of optical transition induced by photon absorption and$B$ is the band edge sharpness constant. The absorption coefficient α can be determined near the

absorption edge using the transmittance data. In crystalline semiconductors crystal momentum is conserved and electron transitions obey well defined selection rules with $\gamma = \frac{1}{2}, \frac{3}{2}$, 2 and 3 corresponding to direct allowed, direct forbidden, indirect allowed and indirect forbidden transitions, respectively. As $SnO_2$is a direct band gap semiconductor, the value of E_g can be obtained from the plot of $(\alpha h\nu)^2$ versus $h\nu$ [21] in the region of high absorption and the extrapolation of the linear region to zero.
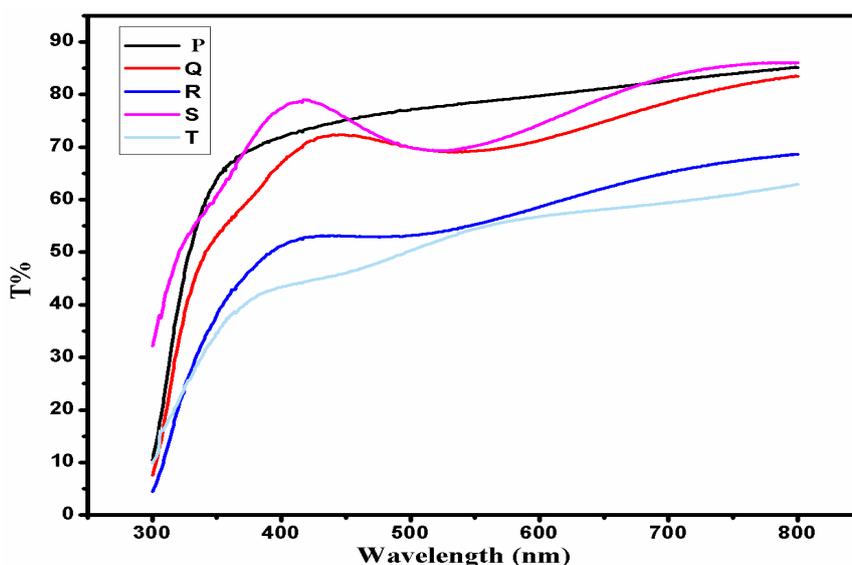

Fig. 3. Transmittance spectrum of SnO$_2$ thin films prepared at different substrate temperatures:(P) 375^{0}C, (Q) 400^{0}C, (R) 430^{0}C, (S) 460^{0}C, (T) 490^{0}C

The observed band gap values and the percentage of the transmittance and refractive index of the film are given in Table 1. The SnO_2nanocrystalline films show an average transmittance of 83%. On the visible region, average transmittance is found to decrease with increase in substrate temperature. The transmittance of the film depends upon the packing density of the film and its surface roughness. Scattering effect is less because of their smaller grain size due to which they exhibit higher transmittance as compared to the heated films with larger

size. The band gap value calculated for all the films are higher than that of the bulk material (3.62eV). It is found that the optical bandgap energy decreases with increase in substrate temperature. As the substrate temperature increased from 460 to 490^{0}C an increase in optical bandgap is observed. The decrease in bandgap with increase in substrate temperature can be attributed to the reduction of oxygen deficiency and approach of film composition towards stoichiometry which is ascertained by X-ray diffraction studies.

Table 1.   Physical parameters of spray pyrolytically grown SnO$_2$ thin films at different substrate temperatures

Sample	Substrate temperature (^{0}C)	T% @550nm	Particle size (nm)	Band gap (eV)	Refractive index@ 550nm	Sheet resistance (kΩ/square)	Figure of merit
P	370	83.5	-	3.954	1.678	4709.4	3.50E+12
Q	400	72.5	8.99	3.947	1.859	93.881	4.31E+13
R	430	71.6	9.23	3.922	1.832	56.764	6.30E+13
S	460	67.8	10.55	3.854	2.112	32.292	6.41E+13
T	490	74.7	16.48	3.900	1.859	8.759	6.23E+14

The bandgap of the as prepared SnO$_2$ nanoparticles is larger than the value of bulk. This can be due to nanostructured nature of the film as observed from XRD

results. In nanostructured particles, charges are localized in individual nanocrystals which results in an increase in bandgap energy. In bulk materials, particles are more

densely packed resulting in overlapping of orbital. But in nanostructured thin films the number of particles is restricted and degree of orbital overlapping is maximum resulting more or less discrete energy states and thus account for the increase in bandgap compared to bulk material.

3.4. Raman studies

Tin oxide has a tetragonal rutile crystalline structure known in its mineral form as cassiterite with point group D_{4h}^{14} and space group P_4^2/mnm. The unit cell consists of two metal atoms and four oxygen atoms. Each metal atom is situated amidst six oxygen atoms which approximately form the corners of a regular octahedron. Oxygen atoms are surrounded by three tin atoms which approximately form the corners of an equilateral triangle. Lattice parameters   a = b = 0.4737nm, c = 0.3186 nm. Ionic radii of O^{2-} and Sn^{4+} are 0.140 and 0.714 nm, respectively.

Fig. 4 shows Micro Raman spectra of SnO_2nanocrystalline thin film samples at various substrate temperatures. The peaks around 396, 785 and 634 cm^{-1} correspond to A_{2g}, A_{1g} and B_{2g}. These peaks further confirm that the as synthesized SnO_2nanocrystalline thin films possess the characteristics of the tetragonal rutile structure. The peak at 634 cm^{-1} is absent in sample P. The XRD results indicate that sample P prepared at a substrate temperature 370^{0}C is almost amorphous and no peak corresponding to SnO_2 is observed for it. A spectral feature centred at 560cm^{-1} is observed for all samples. This band is not normally observed in Raman spectrum of single crystal and polycrystalline SnO_2 and is attributed to the effect of surface phonon modes which dominates when the crystalline size is in the nano regime [22]. So, it can be concluded as a band arising purely from size effect. With

the decrease of crystal size the ratio of surface atoms versus volume atoms increases and thus the contribution of surface phonon increases compared to that from volume phonon [23]. The Raman band at 317 cm^{-1} correspond to IR active $E_u(3)TO$ mode. This situation is similar to the one directly reported by Liu et al for rutile SnO_2nanorods [24]. Samples P, Q and S showed Raman peak at 397cm^{-1} which is the Raman inactive A_{2g} mode.[25]. The mode A_{2g} is related to linear $O - Sn -O$ base which turns around the vertical axis of Sn. The Raman mode A_{2g} is related to vacant lattice position and local lattice disorders that can lead to a change in bond length and space symmetry reduction of D^{14} and serious lattice distortion. The XRD results of as prepared sample indicated the presence of local lattice disorder, vacant lattice sites and oxygen vacancies. It is worth noting that the E_g mode (474 cm^{-1}) is much more broadened in all samples P, Q, R and S. The corresponding peak is absent for sample T. E_g mode is the result of two oxygen atoms vibrating parallel to C-axis but in opposite direction. This shows that E_g is much more sensitive to oxygen vacancies than other modes [26, 27]. Thus E_g mode indicates the existence of oxygen vacancies. SnO_2 films deposited by spray pyrolysis technique are susceptible to oxygen deficiencies. The XRD result shows that as substrate temperature increases, the grain size increases and oxygen vacancies decreases. Sample P showed a Raman peak at 702 cm^{-1} which is attributed to modes activated by disorder. In theory this band can be attributed to disorder activation of A_{2u} IR active and Raman forbidden mode. The result of micro-Raman analysis of SnO_2 nanocrystalline thin films shows that Raman spectrum is sensitively dependent on the surface disorder such as oxygen defects and composition in the surface region.
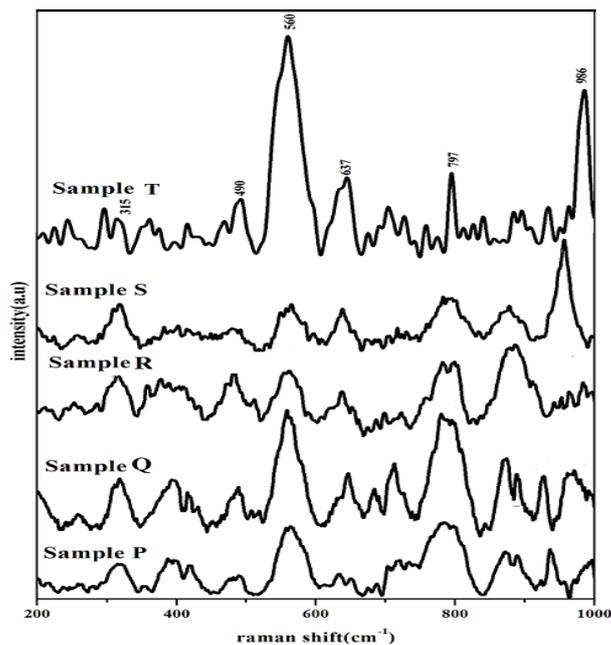

Fig. 4. Micro-Raman spectrum of spray pyrolytically grown SnO_2 thin film samples at different substrate temperatures: (P) 375^{0}C, (Q) 400^{0}C, (R) 430^{0}C, (S) 460^{0}C, (T) 490^{0}C

In a disordered crystal, imperfections modify its symmetry, preventing atoms from vibrating in phase and preventing their displacements to be correlated. Changes in the crystal's local symmetry produce changes in some of the components of the polarisability tensor, even for usually forbidden vibration modes, i.e; due to the loss in long range order of phonons and the Raman spectrum should resemble the phonon density of states. Abello and his co-workers [28] proposed that the relaxation of the k=0 selection rule is progressive when the rate of disorder increases or the size decreases, and infrared (IR) modes can become weakly active when the structural changes induced by disorder and size effects take place. And also, it is well known that in an infinite perfect crystal only the phonons near the center of the Brillouin zone (BZ) contribute to the scattering of incident radiation due to the momentum conservation rule between phonons and incident light. As the crystallite is reduced to nanoscale, the phonon scattering will not be limited to the center of the Brillouin zone, and phonon dispersion near the

centerof Brillouin zone must also be considered. As a result, the symmetry-forbidden modes will be observed.

In a nanoparticle the lowest frequency acoustic like vibrations are in the range of a few wave numbers (cm^{-1}). The low frequency Raman mode of SnO$_2$ thin film samples for various substrate temperatures is shown in Fig 5. The main band appears around 6 cm^{-1}, 67 cm^{-1} and 87 cm^{-1} with slight change in peak position. The peak at 87 cm^{-1} corresponds to B$_{1g}$ mode. The appearance of the low-frequency Raman peaks reminds us of the low-frequency Raman peaks of a spherical particle by Daval et al, [29] Fujii et al., [30]Tanaka et al, [31] and Liu et al [32] who observed low-frequency Raman scattering from localized acoustic vibrations of spherical clusters embedded in glass matrix or porous Si. They have theoretically studied and experimentally confirmed the vibration eigen frequencies of spherical particles by Lamb theory under stress free boundary. Raman peaks that appeared in the low-frequency region may be due to an elastic vibration of the nanocrystals itself, i.e., the confined acoustic phonon modes.
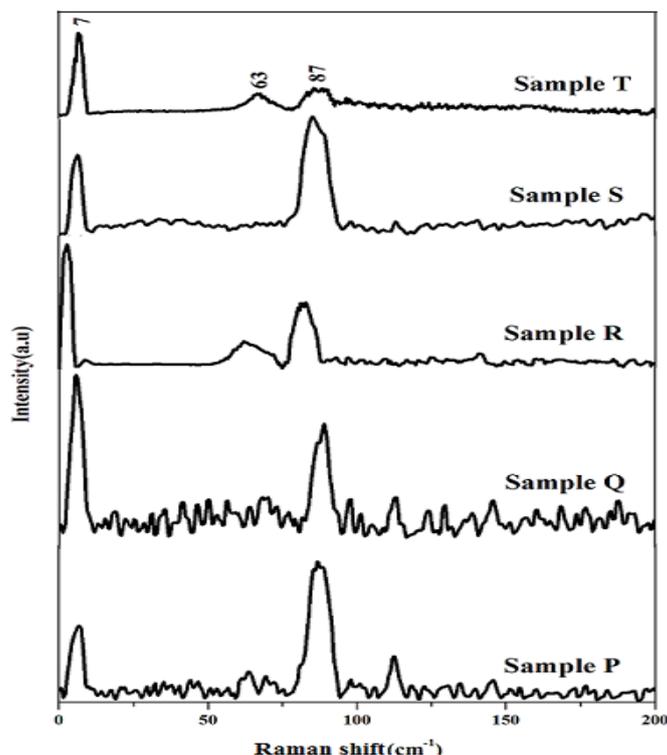

Fig. 5. Low frequency Raman spectrum of SnO$_2$ thin film samples at different substrate temperatures: (P) 375^{0}C, (Q) 400^{0}C, (R) 430^{0}C, (S) 460^{0}C, (T) 490^{0}C

3.5. FTIR studies

The chemical bonds and oxygen related defects were studied by FTIR spectrometer. The IR techniques can

reveal local structure information of amorphous and poorly crystallized samples. Fig. 6 shows the IR spectrum of nanocrystalline SnO$_2$ thin films prepared at different substrate temperatures.

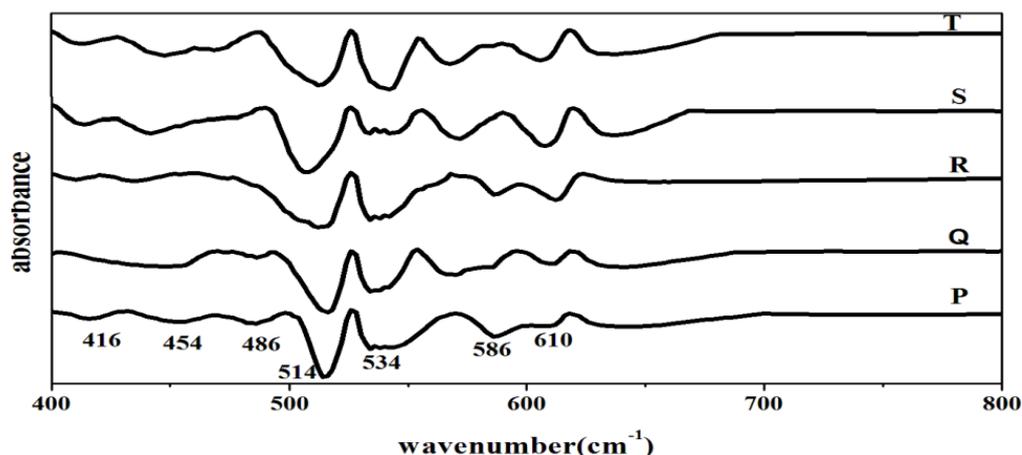*Fig. 6. FTIR spectrums of spraypyrolytically grown SnO₂ thin film samples in the range400-800 cm⁻¹at different substrate temperatures: (P) 375⁰C, (Q) 400⁰C, (R) 430⁰C, (S) 460⁰C, (T) 490⁰C*

The vibrational modes shown by samples are tabulated and are given in Table 2. It can be seen that the two fundamental IR bands at 646 and 480cm^{-1} corresponds to A_{2g} and E_g vibration modes which are in good agreement with the values for rutile bulk SnO₂. The peak at 413cm^{-1} is considered to be the fundamental IR mode A_{2g} at 398cm^{-1} with a minor shift. The spectral feature at 454cm^{-1} could be related to the presence of oxygen vacancies that make the otherwise Raman forbidden A_{2g} mode allowed due to reduced symmetry. Scott [33] has applied Matossi's force constant model [34] on SnO₂ and derived for the frequency of the A_{2g} mode a value of 455cm^{-1}. This agrees well within limits of the model with the result by Yu et al [35] and supports the assumption that oxygen vacancies are responsible for the emergence of that line. A band centered at (606-612cm^{-1}) is observed in sample Q,R,S and T but is absent in sample P. The infrared feature of SnO₂ thin film at 610cm^{-1} can be assigned to Sn-O stretching mode. The appearance of this band corresponding to E_u mode of cassiterite indicates that as substrate temperature increases the small grains become larger and the amorphous phase transformed into crystalline phase. The main feature of XRD spectra is the narrowing of XRD peaks as the substrate temperature is increased, which reveals that there is an increase in grain size and higher crystalline quality.

Table 2. Vibrational modes shown by nanocrystalline SnO₂ thin films prepared by spraypyrolysis

Vibrational modes		Sample				
		P	Q	R	S	T
A_{1g}	634cm^{-1}	646	648	648	648	648
E_u	605 cm^{-1}		606	612	608	606
	S1	586	570	586, 568	570	566
	S2	534	534	534	534	534
	A_{2u}	516	512	516	506	512
E_g	475 cm^{-1}	480	491	474	480	468
		454	448	436	442	448
A_{2g}	398 cm^{-1}	416	-	410	412	418

Two interesting features of SnO₂ thin film is observed around 468-475cm^{-1} and 606-619cm^{-1} which are assigned to O-Sn-O and Sn-O stretching vibrations, respectively. In order to get a better insight into oxygen vacancy (V_0^{2+}) a systematic study on the features on FTIR is done. There are two lattice sites for oxygen (u, u, 0) and (0.5+u, 0.5-u, 0.5) in SnO₂ lattice, which correspond to the oxygen in the group of O-Sn-O andSn-O. So the vibrational features of O-Sn-O and Sn-O can reflect the defects in SnO₂ lattice, especially on the oxygen site. For V_0^{2+}, it is easy to occur on the group of O-Sn-O because of different bond lengths (O-Sn-O = 2.597A^0, Sn-O = 2.053 A^0). The presence of V_0^{2+} can deform the O-Sn-O group to O-Sn-V$_o$ which is seemingly as a deformed Sn-O group. It is that the repulsive force between Sn^{4+} and V_0^{2+} (O^{2-}- Sn^{4+}- V_0^{2+}) has a compression effect on the deformation of Sn-O. The compressed Sn-O bond shows an increased vibration frequency at 644 cm^{-1} in FTIR according to the harmonic oscillator model. Thus the feature at 645 cm^{-1} can be identified as the indication of presence of oxygen vacancies [36].

FTIR spectrum in the range 1000-4000 cm^{-1} is shown in Fig 7. Water is responsible for a large component of hydroxyl stretching made in the range of 3700-3200 cm^{-1} with maximum at about 3500 cm^{-1}. The molecular water deformation mode locates at about 1640 cm^{-1}. It is known that dehydration from SnO_2 particles occur via condensation of surface hydroxyl group on [100] and [101] plane. Hydroxyl group condensation on their planes will lead to the bridges. The stretching mode of mentioned bridge is at about 1450 cm^{-1}.
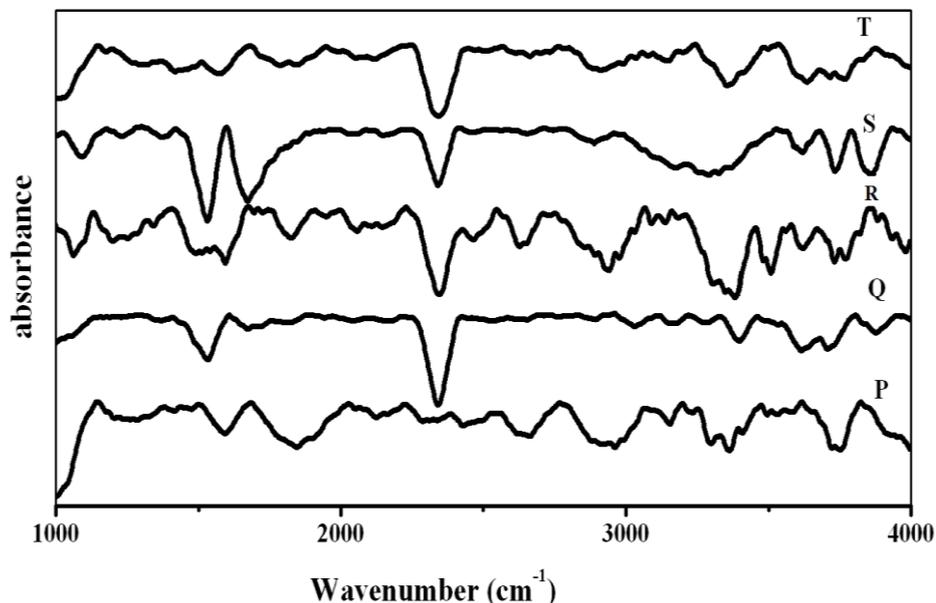

Fig. 7. FTIR spectrum of SnO_2 thin film samples in the range 1000-4000cm^{-1} at different substrate temperatures: (P) 375^{0}C, (Q) 400^{0}C, (R) 430^{0}C, (S) 460^{0}C, (T) 490^{0}C

4. Conclusion

High quality SnO_2 nanocrystalline thin films were prepared on glass by a simple and inexpensive spray pyrolysis technique. The XRD studies revealed that all the films are polycrystalline in nature with rutile type structure. Crystallite size determination based on the Scherrer method showed that all the samples were in the nanometric range. The optical direct bandgap lies in the range between 3.85 to 3.95eV. Transmission spectra showed particle size dependent blue shift in the energy band which may be ascribed to the quantum confinement effect. A systematic Raman study of SnO_2 nanocrystalline thin films has been reported. Three fundamental modes of rutile SnO_2 bulk were observed at 396, 785, 634 cm^{-1} corresponding to A_{2g}, A_{1g} and B_{2g} modes. Four new peaks, 397, 560 and 702 cm^{-1} are observed in SnO_2 thin films. The first two modes correspond to IR active $E_u(3)$ TO mode and Raman inactive A_{2g} mode respectively. The band at 702 cm^{-1} is attributed to disorder activated mode. The spectral feature at 560 cm^{-1} is the result of size effect of SnO_2 nanocrystalline thin films.

References

[1] M. S. Gudiksen, L. J. Lauhon, J. Wang, D. Smith, C. M. Luber, Nature **415**, 617 (2002).
[2] Abdul Rasheed Paloly, M. Satheesh, M. Junaid Bushiri, Ceramics International **45**, 11032 (2019).
[3] Abdul Rasheed Paloly, M. Satheesh, M. Carmen Martínez-Tomás, Vicente Muñoz-Sanjosé, M. Junaid Bushiri, Applied Surface Science **357**, 915 (2015).
[4] A. Henglein, Chem. Rev. **89**, 1861 (1989).
[5] H. Weller, Adv.Mater. **32**, 41(1993).
[6] A. Dieguez, A. Romano Rodriguez, A.Vilaand, J. R. Morant, J. Appl. Phys. **90**, 1550 (2001).
[7] H. Ogawa, A. Abe, M. S. Hayakawa, J. Electrochem. Soc. **128**, 2020 (1981).
[8] Z. M. Jarzebski, J. P. Marton, J. Electrochem. Soc. **123**, 299c (1976).
[9] S. C. Ray, M. K. Karanjai, D. Dasgupta, Thin Solid Films **30**, 221 (1997).
[10] P. Siciliano. Sens. Actuators B**70**, 153 (2000).
[11] D. M. Mukhamedshina, N. B. Beisenkhanov, K. A. Mit, I. V. Valitova, V. A. Bolvin, Thin Solid Films **495**, 316 (2006).
[12] K. S. Shamala, L. C. S.Murthy, K. Narasimha Rao, Bull. Mater. Sci. **27**, 295 (2004).
[13] E. Elangovan, K. Ramamurthi, Appl. Surf. Sci. **249**, 183 (2005).

[14] Saji Chacko, M. J. Bushiri, V. K. Vaidyan, J. Phys. D: Appl. Phys. **39**, 4540 (2006).

[15] J. Shadia, Ikhmayies, N. Riyad, Ahamed-Bitar, Appl. Surf. Sci. **255**, 2627 (2008).

[16] E. Elangovan, K. Ramamurthi, Appl. Surf. Sci **249**, 183 (2005).

[17] Vitor Baranauskas, Marcio Fontana, Zhao Jing Guo, Helder Jose Ceagioli, Alfredo CarlosPeterlevitz, Sensors and Actuators B**107**, 474 (2005).

[18] S. F. Kistler, in Wettability, Surfactant Science Series **49**, J. C. Berg, Ed. Dekker, New York, chap. 6 (1993).

[19] F. Gu, S. F. Wang, M. K. Lu, G. J. Zhou, D. Xu, D. R. Yuan. J. Phys. Chem. B **108**, 8119(2004).

[20] Z. W. Chen, J. K. L. Lai, C. H. Shek, Physical Review B **70**, 165314 (2004).

[21] J. Tauc, Amorphous and liquid semiconductors, Plenum, London 159 (1974).

[22] J. Zuo, C. Xu, X. Liu, C. Wang, Y. Hu, Y. J. Qian, Appl. Phys. **75**, 1835 (1994).

[23] L. Abello, B. Bochu, A. Gaskov, S. Koudryavtseva, G. Lucazeau, M. Roumyantseva. J. Solid State Chem. **135**, 78 (1998).

[24] Y. K. Liu, C. L. Zheng, W. Z. Wang, C. R. Yin, G. H. Wang, Adv. Mater.**13**, 1883 (2001).

[25] R. S. Katiyar, P. Dawson, M. M. Hargreave, G. R. Wilkinson, J. Phys. C .**4**, 2421 (1971).

[26] S. H. Sun, G. W. Meng, G. X. Zhang, T. Gao, B. Y. Geng, L. D. Zhang, J. Zuo, Chemical Physics Letters **376**, 103 (2003).

[27] J. C. Paker, R. W. Siegel. Appl. Phys. Lett. **57**, 943 (1990).

[28] L. Abello, B. Bochu, A. Gaskov, S. Koudryavtseva, G. Lucazeau, M. Roumyantseva. J. Solid State Chem. **135**, 78 (1998).

[29] E. Duval, A. Boukenter, B. Champagnon. Phys. Rev. Lett. **56**, 2052 (1986).

[30] M. Fujii, Y. Kanzawa, S. Hayashi, K. Yamamoto, Phys. Rev. B. **44**, 6243 (1991).

[31] A. Tanaka, S. Onari,T. Arai, Phys. Rev. B **47**, 1237 (1993).

[32] F. Q. Liu et al., Phys. Rev. Lett. **76**, 60 (1996).

[33] J. F. Scott, J. Chem. Phys. **53**, 852 (1970).

[34] F. Matossi. J. Chem. Phys. **13**, 1543 (1951).

[35] K. N. Yu, Y. Xiong, Y. Liu, C. Xiong, Phys. Rev. B **55**, 2666 (1997).

[36] B. Zhang, Y. Tian, J. X. Zhang, W. Cai, Appl. Phys. Lett. **98**, 021906 (2011).

_____

*Corresponding author: kurian.vaidyan@gmail.com